The Tyrosine Photophysics of a Primase-Derived Peptide Are Sensitive to the Peptide's Zinc-Bound State: Proof That the Bacterial Primase Hypothetical Zinc Finger Sequence Binds Zinc[†]

Mark A. Griep,* Betsy J. Adkins, Daniel Hromas, Scott Johnson, and Jennifer Miller

Department of Chemistry and the Center for Biotechnology, University of Nebraska, Lincoln, Nebraska 68588-0304

Received May 30, 1996; Revised Manuscript Received November 6, 1996[⊗]

ABSTRACT: A 35-amino acid peptide corresponding to the putative "zinc finger" sequence of primase was prepared to study its zinc binding properties. When zinc was added to the peptide, it was found that the fluorescence quantum yield of the single tyrosine increased by 46% and the average lifetime by 34%. The binding stoichiometry was one zinc per peptide. Below pH 6.0 and above pH 8.5, the zinc−peptide binding affinity was less than 1 μM and could be accurately determined. Interpolation from those binding constants suggested that the affinity at pH 7.5 was between 10 and 100 nM. The absorption spectrum of the cobalt(II)−peptide complex was consistent with tetrahedral metal coordination by three sulfur and one imidazole nitrogen ligands. The peptide affinity for cobalt was less than for zinc, indicating metal specificity. Analysis of the fluorescence intensity pH profile, circular dichroism spectra, the effect of extrinsic quenchers indicated that at neutral pH (1) the free peptide folded up into a structure to place the tyrosine in an environment protected from solvent, (2) the peptide bound zinc via its three cysteines and one of its histidines resulting in little change to the polypeptide secondary structure or to the tyrosine solvent accessibility, and (3) when the peptide bound zinc, it bound directly to or caused the immobilization of the groups that had been intramolecularly collisionally quenching the tyrosine which resulted in the observed increases in tyrosine quantum yield and lifetime.

Primase plays the central role at the replication fork during DNA synthesis (Kornberg & Baker, 1992; Marians, 1992).[1] It is the single-stranded DNA-dependent RNA polymerase that initiates DNA polymer synthesis once for the leading strand DNA polymerase and multiple times for the lagging strand DNA polymerase. Leading strand synthesis is initiated by primase at the replication origin after origin-specific proteins and enzymes have opened the duplex DNA at that site. After a replication fork has been created, lagging strand synthesis is initiated by primase once every 500−2000 nucleotides at the replication fork. At the fork, DnaB helicase unwinds the duplex DNA to create the single-stranded DNA that is the template for primase and then the lagging strand DNA polymerase. The termination of DNA replication also involves primase (Grompe et al., 1991) but in a manner yet to be established.

Even though the 581-amino acid sequence of *Escherichia coli* primase is known (Burton et al., 1983) and even though there are several primase-overproducing strains available, there is no high-resolution primase structure upon which to base structure/function studies. Most of the information concerning the functional domains of primase can be placed within the framework of recent sequence analyses of bacterial and bacteriophage primases and bacterial and eukaryotic RNA polymerases (Ilyina et al., 1992; Versalovic & Lupski, 1993). Several regions of adjacent invariant residues have been identified and functions for some of the motifs have been hypothesized or proven.

The most highly conserved sequence in primase is a putative zinc finger located at roughly residues 35−70 (Griep, 1995; Ilyina et al., 1992; Versalovic & Lupski, 1993). Even though the term zinc finger was coined for a specific instance (Miller et al., 1985), the term has evolved to include any moderate length of polypeptide that is capable of binding one or two zincs and usually has discrete functionality (Klug & Schwabe, 1995; Schmiedeskamp & Klevit, 1994; Vallee & Auld, 1993). *E. coli* primase binds one zinc per polypeptide (Stamford et al., 1992), and it is ligated by three cysteine sulfhydryls (Griep & Lokey, 1996) consistent with the sequence prediction. One role of the zinc is to prevent inhibitory disulfide bonds from forming (Griep & Lokey, 1996). This may be a common protein role of this biologically abundant, low redox active metal (Bertini & Luchinat, 1994). The high sequence conservation of residues adjacent to the zinc ligating residues suggests that they also play an important role in enzyme structure or function. Potential roles include protein-specific binding or DNA sequence-specific binding. In fact, excellent evidence has been presented that the role of the zinc in sequence-related bacteriophage T7 primase/helicase has to do with primer initiation sequence specificity (Bernstein & Richardson, 1988; Mendelman et al., 1994).

In an *E. coli* lagging strand DNA synthesis system, the initiating and rate-limiting event involves primer synthesis

[†] This work was supported by funds from the UNL Center for Biotechnology, the Council for Tobacco Research (#3581), and the National Science Foundation (OSR-9255225) to M.A.G. and by funds from the Howard Hughes Research Foundation Undergraduate Research Program to B.J.A.

* Author to whom correspondence should be addressed. Tel: (402) 472-3429.

[⊗] Abstract published in *Advance ACS Abstracts,* January 1, 1997.

[1] Abbreviations: CHES, 2-(*N*-cyclohexylamino)ethanesulfonic acid; DTT, dithiothreitol; HEPES, *N*-(2-hydroxyethyl)piperazine-*N*′-(2-ethanesulfonic acid); PIPES, piperazine-*N*,*N*′-bis(2-ethanesulfonic acid); Tris, tris(hydroxymethyl)aminomethane.

S0006-2960(96)01277-9 CCC: $14.00

Table 1: Fluorescence Lifetimes of *N*-Acetyltyrosinamide[a]

1[b]	3[c]	2-component fit							
χ^2	χ^2	χ^2	a_1	τ_1 (ns)	a_2	τ_2 (ns)	$<\tau>$ (ns)	conditions	reference
14	3.1	2.6	0.96	1.52	0.04	0.21	1.47	25 °C, ex 280, all em	this work
			0.86	2.22	0.14	0.93	2.04	5 °C, ex 284, em 302	Laws et al., 1986
86		2.8	0.65	1.657	0.35	0.111	1.12	20 °C, ex 286, em 300 interference filter	Lakowicz et al., 1987

[a] The values from this work were obtained as described under Experimental Procedures. The χ^2 residuals goodness-of-fit values were determined for 1-, 2-, and 3-component fits. The lifetimes and amplitudes for our best fit are shown. [b] 1-Component fit. [c] 3-Component fit.

(Wu et al., 1992; Zechner et al., 1992). In a study of primase activity alone, the rate-limiting step was identified as either formation of the first phosphodiester bond or, more likely, a step preceding it (Swart & Griep, 1995). Understanding how the structure of the primase zinc finger achieves trinucleotide-specific initiation is therefore central to understanding this signature primase function. As the first step toward elucidating the structural role of the zinc in primase, we chose to have a peptide synthesized with the most highly conserved residues in the sequence. The fluorescence intensity of the single tyrosine has proven to be a sensitive monitor of the metal-bound state of this peptide.

EXPERIMENTAL PROCEDURES:

Peptide Synthesis, Isolation, and Purity. The 35-residue peptide KNFHA LCPFH NEKTP SFTVN GEKQF YHCFG CGAHG was synthesized on an Applied Biosystems 431A Peptide Synthesizer using Fmoc chemistry. The underlined leucine in the sequence signifies the position at which the peptide differs from the *E. coli* residues 34−69. In most bacterial primases, leucine is located at this position but in *E. coli* it is a cysteine. To eliminate anticipated problems that might accrue from this nonessential cysteine the peptide was prepared with the preferred leucine. The crude peptide was separated from synthesis reagents on a preparative C18 column using a 0.5%/min acetonitrile gradient. The peak peptide eluted at 36.8% acetonitrile, very close to the elution concentration of 37% predicted by a program written using published amino acid/C18 partition coefficients (Griep & Mesman, 1995; Sasagawa et al., 1982). Amino acid analysis of the pure peptide indicated that the concentration of each of the expected residues were present to within 8% of the average residue concentration, except serine at 65% of the average and cysteine at 85%. The low recoveries for these residues was typical. Analytical C18 HPLC indicated that the pure peptide consisted of only one eluting species. Matrix-assisted laser desorption mass analysis with a Bruker BenchTOF indicated that the pure peptide was greater than 97% single species and the major contaminants were of much lower molecular weight. Representing less than 3%, the potential fluorescence contributions of these species were ignored.

The concentration of native, denatured and zinc-bound peptide were determined using an extinction coefficient of 1335 M^{-1} cm^{-1} at 280 nm. This value was calculated using an extinction of 11 for each of its five phenylalanines and 1280 for its single tyrosine. It was found that the absorbance spectrum of the peptide did not differ whether it was dissolved in 0.1% trifluoroacetate, in 6 M guanidinium chloride, in pH 7.5 buffered solution, or in the presence of zinc indicating that the same extinction coefficient could be used for each peptide structural state. Unless otherwise stated, the buffer for all experiments was 50 mM HEPES, 100 mM potassium glutamate, pH 7.5, 5 mM DTT.

Fluorescence Steady State Measurements. The steady state fluorescence measurements were made using an Aminco-Bowman 2 spectrofluorimeter controlled by an IBM running OS/2. The sample compartment was maintained at 30.0 ± 0.1 °C and the quartz cuvette was 1.0 × 0.4 cm in size with path lengths half those lengths. The excitation and emission bandwidths were each set at 4 nm during the zinc titration experiments. The emission bandwidth was lowered to 1 nm during the quantum yield and emission spectral measurements. All measurements have been corrected for background fluorescence, dilution effects, and instrumentation effects.

Quantum yields were determined using the relationship $\phi_x = (F_x A_{ref} \phi_{ref})/(F_{ref} A_x)$, where ϕ was quantum yield, A was absorption at the excitation wavelength, F was area under the fluorescence emission curve, and the subscripts x and ref were the unknown and the reference samples (Parker & Rees, 1960). The concentrations of the unknown and reference were adjusted so that their absorbances were less than 0.050 to prevent any inner filter effects (Lakowicz, 1983). The reference quantum yield for *N*-acetyltyrosinamide was 0.14 ± 0.01 (Chen, 1967; Longworth, 1983).

Fluorescence Lifetime Measurements. Tyrosine fluorescence decay lifetimes were obtained by frequency domain analysis at the Aladdin Biofluorescence Center (Aladdin Synchrotron, Stoughton, WI) with the assistance of Gediminas Vidugiris. The main harmonic was pulsed at about 50.3 MHz and the minor harmonic at 3.14 MHz. A monochrometer was used to select an excitation wavelength of 280 nm from the 800 mA radiation, and all light emitted at a 90° angle from the excitation beam was used as the emission signal. The lifetimes were determined relative to a glycogen scattering solution, the concentration of which was chosen to scatter light with an intensity equal to that of the fluorescing sample. The peptide concentration was higher than 50 μM. For each sample, the phase shift and demodulation of the emitted light relative to the absorbed light were measured at nine integrals of the minor harmonic frequency from 6 to 450 MHz. The lifetimes were obtained from these data by the method described by Lakowicz et al. (1987) using the Globals Unlimited software. Basically, these values were fit to a multicomponent equation by a nonlinear least-squares procedure to obtain the amplitude a_i and lifetime τ_i of each fluorescing species i in the sample where the amplitudes were constrained by the relationship $\sum a_i = 1$. Fits to the data were generated assuming one, two, or three species and the goodness-of-fit determined by χ^2. The smaller the χ^2, the better the fit. The mean (amplitude-weighted) lifetime $<\tau>$ was calculated from $\sum a_i \tau_i$.

To establish that the instrumentation could be used to measure tyrosine lifetimes, the control compound *N*-acetyltyrosinamide was tested (Table 1). It had a lifetime that was well-described by a 2-exponential decay with an average

lifetime of 1.47 ns. A biexponential decay has been previously reported for this compound (Lakowicz et al., 1987; Laws et al., 1986) and our component amplitudes and lifetimes were similar but not identical to those previously reported. The difference with the values reported by Laws et al., average 2.04 ns, might be explained by the different temperatures used, 5 versus our 25 °C. The difference with the values reported by Lakowicz et al. was primarily in the amplitudes and not the lifetimes; component 1 amplitude was 0.65 versus our 0.96. The difference might be due to the reference method used, we used glycogen total light scattering. We concluded that synchrotron radiation provided an adequate source of wavelength-selectable light which yielded data with goodness-of-fits as good as reported by others.

Relationship between Fluorescence Quantum Yield and Lifetime. When an excited state fluorophore relaxes to its ground state, it loses energy by radiative and nonradiative processes. The radiative process in our case is fluorescence and the nonradiative processes include vibrational dissipation, intersystem crossing from the excited singlet to the excited triplet state, energy transfer, and dynamic quenching. The average time that the fluorophore spends in the excited state is called the fluorescence lifetime τ and is represented by $\tau = 1/(k_r + \sum k_{nr})$ where k_r and $\sum k_{nr}$ are the first-order rates of the radiative and nonradiative processes. The fluorescence quantum yield ϕ is the fraction of excited state molecules that decay by a radiative process and is determined by $\phi = k_r/(k_r + \sum k_{nr})$. These equations indicate that the relationship between lifetime and quantum yield is $\phi = k_r\tau$. Since both lifetime and quantum yield can be measured, this latter equation allows the determination of k_r. When there are multiple fluorescent species but no information relating them to actual conformational species, the average radiative rate constant can be calculated from the equation $<k_r> = \phi/<\tau>$. Having determined the radiative rate constant, it is possible to determine the average sum of the nonradiative rate constants $<\sum k_{nr}>$ from either of the other relationships.

Dynamic Quenching Measurements. Fluorescence quenching caused by intermolecular quenching agents was analyzed using the Stern and Volmer approach (Stern & Volmer, 1919). Small aliquots from 4 M stocks of potassium iodide, cesium chloride, and acrylamide were added sequentially into peptide (10 μM) solutions containing either 12 μM zinc acetate or 3 mM EDTA, and the fluorescence intensity measured as above. The buffer for these experiments was 50 mM HEPES, 100 mM potassium glutamate, 5 mM DTT, pH 7.5. The iodide and cesium quenching data were analyzed by the equation for collisional quenchers, $F/F_o = 1/(1 + K_{SV}[Q])$, where F was the fluorescence intensity at a given quencher concentration, F_o was the fluorescence intensity in the absence of quencher, K_{SV} was the Stern−Volmer quenching constant, and [Q] was the quencher concentration.

The acrylamide quenching data had to be corrected for the excitation inner filter effect (Lakowicz, 1983) using the relationship $F' = F$ antilog($\epsilon_{ex} l_{ex}$[acrylamide]/2), where F' was the transmittance-corrected fluorescence intensity, F was the fluorescence intensity (corrected for background and dilution as usual), ϵ_{ex} was the acrylamide extinction coefficient at the excitation wavelength (3.51 M^{-1} cm^{-1} at 280 nm), and l_{ex} was the excitation light path length (0.5 cm) (Lakowicz, 1983). There was no need to correct for the emission inner filter effect because the acrylamide extinction coefficient at 305 nm was negligible. Since the acrylamide quenching data demonstrated pronounced upward curvature in a classical Stern−Volmer plot, the data were fit to a modified equation (Eftink & Ghiron, 1976), $F/F_o = 1/(1 + K_{SV}[Q])e^{V[Q]}$, where V represented the static quenching constant and was related to the volume surrounding the fluorophore in which the quenching agent can cause quenching without actually colliding with the fluorophore. The effective volume element was related to the sphere radius r by $V = N_A 4\pi r^3/3$, where N_A was Avogadro's number.

The intermolecular collisional quenching constant was determined from $k_q = K_{SV}/<\tau_0>$, where $<\tau_0>$ was the average fluorescence lifetime in the absence of quencher. This quenching constant contained information about the diffusion collision rate of the fluorophore and quencher, the quenching efficiency of the quencher, $frac_{exposed}$, the fraction of fluorophore that was accessible to the quencher, and size of the macromolecule to which the fluorophore was attached (Johnson & Yguerabide, 1985). The ratio k_q(peptide)/k_q(indole) eliminated the effects from the quenching efficiency and was used to obtain a qualitative assessment of $frac_{exposed}$. The values used for k_q(indole) (Eftink & Ghiron, 1981) were 7.1×10^9 M^{-1} s^{-1} for acrylamide, 6.4×10^9 M^{-1} s^{-1} for iodide, and 1.1×10^9 M^{-1} s^{-1} for cesium.

Circular Dichroism Measurements. The circular dichroism spectra were made using a JASCO J-600 spectropolarimeter (Easton, MD) and were collected and analyzed using the company software. The bandwidth was 1 nm, the sensitivity was 20 mdeg/fs, the time constant was 16 s, the scanning resolution was 0.2 nm, and the scan speed was 5 nm/min. Prior to each scan, the background was set using the appropriately pH-adjusted solvent. Each spectrum represents the average of four scans which were then smoothed over a 1-nm range. The samples were placed in a cuvette with a 0.1 cm path length.

Data Equation Fitting. Data from all experiments were fit to their respective equations by the nonlinear least-squares approach using Excel 5.0 (Microsoft Corporation) and the FIT! program (WindowChem Software, Fairfield, CA). Equations used were chosen so that the response values were correctly weighted. As an example, the extrinsic quenching data were fit to the equation $F = F_o/(1 + K_{SV}[Q])$ rather than the usual Stern−Volmer equation $F_o/F = 1 + K_{SV}[Q]$ because the signal response was F and not $1/F$ (Eftink, 1991).

RESULTS

Primase Zinc Finger Sequence/Structure Analysis. The goal of this study was to establish whether the predicted zinc ligating sequence of primase could bind zinc. Previous sequence analyses using fewer primase sequences (Griep, 1995; Ilyina et al., 1992; Versalovic & Lupski, 1993) determined that bacterial and bacteriophage primases have similar arrangements of identical and conserved residues within their linear sequences. The residues with the highest degree of conservation were near the amino-terminus and consisted of a putative zinc binding sequence. When the currently available bacterial sequences were aligned (Figure 1), it indicated that the most highly conserved residues were those that occur between the putative zinc binding residues cysteines 40 and 64 of the sequence from *E. coli*. The putative zinc finger sequence from the bacterial primases

Primary Structures

```
E. coli   30-KKQGKNFHAC CPFHNEKTPSFTVNGEKQFYHCFGC GAHGNAIDFLM
S. typh   30-KKQGKNYHAC CPFHNEKTPSFTVNGEKQFYHCFGC GAHGNAIDFLM
H. infl   30-KKAGRDYQAC CPFHHEKTPSFTVSQKKQFYHCFGC GAHGNAISFLM
L. mono   29-KKQGRNYSGL CPFHGEKTPSFSVSPEKQMFHCFGC GKGGNVFSFLM
B. subt   30-KKQGRNYFGL CPFHGESTPSFSVSPDKQIFHCFGC GAGGNVFSFLR
C. acet   31-KRTGRNYSGL CPFHHEKTPSFSVSQDKQIYKCFGC GEAGNVITFVM
L. lact   29-SRTGKNYIGL CPFHGEKTPSFNVNAEKGFYHCFGC GRSGDAIEFLK
Synecho   28-KKRGKDFVGL CPFHDDKSPSFTVSPAKQFYYCFSC GAGGNPIKFLM
M. xant   30-KKAGREWKAC CPFHQEKTPSFYVVPEKRFYFCHGC RASGDAVSFVQ
R. prow   28-TRKSSNYVGL CPFHQEKTPSFTVSDSKRFFYCFGC KASGDVIKFTS
M. geni   29-QTKGNSLLAL CPFHDDKNPSMSISSSKNIFKCWAC NAAGNGIAFIQ
#aminoacids 4352444922 11115223112423661432413314 44412436145
consensus   KKxGRNYxGL CPFHxEKTPSFTVSxxKQFYxCFGC GxxGNAIxFLx
                  K   AC            S N     F          V
Classic zinc finger consensus          (F/Y)xCxxC xxxF
```

Secondary Structure Predictions

```
E. coli     hhh.tt.... .TT.....TT..tttt.BBBBBBtt .tttHHHHHH
S. typh     hhhhTT.... .TT.....TT..tttt.BBBBBBtt .ttttHHHHHH
H. infl     hhh.tt.... .TT.....TT..tttt.BBBBBBtt .ttttHHHHHH
L. mono     hhh.TTt... .hhhhhhhTThhhhhhhhBBBBBBtt .ttttHHHHHH
B. subt     hhh.TTtt.. .TT.tt..Ttt...TTtBBBBBBtt .TTttBBBBBh
C. acet     hhttTTTTT. ..hhhhhhTtt...TT BBBBBBtt .....BBBBBB
L. lact     .tttTT.... .TT.tt..TThhhhhhh.BBBBBtt tTTttHHHHHH
Synecho     .tttttBBBB BBB.TTttTT....tt.BBBBBBtt .TTtt.BBBBB
M. xant     hhhhhhhhhh hhhhhhhh.BBBBB...BBBBBBtt .ttttBBBBBB
R. prow     ..ttTT.... .hhhhhhhTT...TTTtBBBBBB.. .tthhhhhhh.
M. geni     BBBTTt.bbbbbbb.TTTTTT...tTTtthhhhhhhhhhhhttBBBBB

consensus   hhh.TT.... .TT.....TT....TT.BBBBBBtt .tttt......
```

FIGURE 1: Sequence alignment and secondary structure predictions for eleven bacterial primase zinc fingers. The number of different amino acids found at each position is indicated below the alignment. The consensus for both primary and secondary structure was derived from residues that appeared in more than two-thirds of the sequences and for the primary structure where two residues were present at roughly equal frequency. The secondary structure algorithm was adapted from known secondary structures in globular proteins (Chou & Fasman, 1974) and calculated using the Wisconsin Genetics Database protein structure program (Group, 1994). The algorithm was applied to the entire protein sequence but only the structure predictions for the portion of primase containing the zinc finger is shown. The structure predictions are reported as "B" or "b" for β strand, "H" or "h" for helix, and "T" or "t" for reverse turn. An upper case letter indicates a greater likelihood for the indicated type of structure than a lower case letter. The bacterial sequences were obtained from GenBank and have the following acquisition numbers: *E. coli*, J01687; *Salmonella typhimurium*, M14427; *Haemophilus influenzae*, L11044; *Listeria monocytogenes*, U13165; *Bacillus subtilis*, X03897; *Clostridium acetobutylicum*, Z23080; *Lactococcus lactis*, D10168; *Synechococcus*, X94247; *Myxococcus xanthus*, U20669; *Rickettsia prowazekii*, M95860; and *Mycoplasma genitalium*, U39703.

was Cys-X_2-His-X_{15}-Cys-X_2-Cys placing it in a zinc finger family with eukaryotic viral primase/helicases [Table IV of Mendelman et al. (1994)]. Besides the invariant putative zinc ligating residues there were seven other invariant residues between the zinc ligating ones, yielding 44% identity in this region, the highest cluster of identical residues within primase.

There is such a strong correlation between the conserved residues with the sequence of eukaryotic transcription factor zinc fingers (i.e., "classical" zinc fingers) and their three-dimensional structure that it proved possible to predict their tertiary structure from their sequence (Berg, 1995). This was achieved by searching a protein structure database for motifs resembling both halves of zinc binding sequence. This same approach was applied to the bacterial primase zinc binding sequence to determine whether there was precedence for metal binding by its two halves. The Swiss-Prot ExPASy ScanProsite Tool was used to search the Swiss-Prot database for amino acid sequences that resembled the two halves of the finger. When the sequence Cys-X-Phe-His was searched, it was found to occur in over 300 proteins. When the sequence Cys-Pro-X-His was searched, it was found in about 570 proteins. Out of these sequence matches, ten were for bacterial primases. Of the remaining sequence matches, very few were metalloproteins. In those matches that were metalloproteins, there was no instance in which the cysteine and histidine were both ligated to the metal. There were several protein matches in which the cysteine was disulfide bonded and several others in which the cysteine was ligated to an iron−sulfur cluster. The only instance in which the histidine played a role was in bovine carboxypeptidase B. In this protein, the histidine is bound to the catalytic zinc while the cysteine from the matched sequence participated in a disulfide bond.

The second half of the bacterial primase zinc binding motif, (Phe/Tyr)-Cys-X-(Ala/Gly/Ser)-Cys and (Phe/Tyr)-Cys-(His/Phe/Tyr)-X-Cys, generated over 300 matches. About one-half of the matches were to eukaryotic transcription factors containing the classical zinc finger motif or to steroid receptors containing their type of zinc finger motif. The rest were to non-metal containing proteins. The first half of the classical zinc finger which is similar in sequence to the second half of the primase zinc finger has a structure consisting of two antiparallel β strands in which the zinc ligating residues are located at the turn and the conserved large nonpolar residues are located in the nonpolar interior of the folded structure (Berg, 1995). From the above analysis, it was expected that the structure of the primase zinc finger would be different from other zinc fingers. Another confirmation that the primase zinc finger structure was different from classical zinc fingers came from secondary structure predictions (Figure 1) based on Chou and Fasman's data for globular proteins (Chou & Fasman, 1974). The linear amino acid sequence of the primase zinc binding region was predicted to have a β strand where the classical zinc finger has an α helix (Figure 1). The algorithm also predicted that the invariant glycines and prolines correlated to reverse turns but that no particular structure was strongly predicted for the residues surrounding the first half of the zinc finger.

To test whether this region of primase could bind a metal, a peptide based on the *E. coli* primase sequence was synthesized which included five residues before the first zinc binding residue and four residues after the last. With its five phenylalanines, two alanines and prolines, and single leucine, valine, and tyrosine, the peptide was very nonpolar. To enhance solubility, the residues preceding and following the outermost ligating residues were chosen to include most of the flanking highly conserved residues and some charged residues. The carboxyl-terminal glycine was chosen instead of the histidine to prevent isomerization of a terminal histidine during post-synthetic purification.

Peptide Absorbance and Fluorescence. The normalized absorption spectrum of this peptide (Figure 2) showed that the single tyrosine and five phenylalanines dominated. This spectrum was very similar to that calculated using equiresidue absorption spectra of standard solutions of *N*-acetylphenylalaninamide and *N*-acetyltyrosinamide (data not shown), indicating that the electronic structures of the tyrosine and phenylalanines in the peptide were not significantly altered by their adjacent residues. From this it was concluded that tyrosine absorption could be selected by excitation above 280 nm since *N*-acetylphenylalaninamide does not absorb significantly above that wavelength.

The fluorescence excitation and emission spectra of the free and zinc-bound peptide (Figure 2) were characteristic

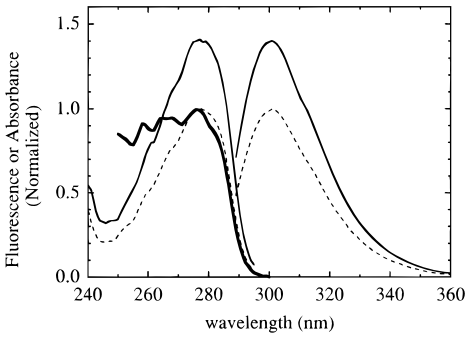

FIGURE 2: Absorption and fluorescence spectra of primase zinc finger peptide. The free (dashed lines) and zinc-bound (continuous lines) peptide fluorescence spectra were normalized to the free peptide intensities at its excitation and emission maxima of 278 and 301 nm, respectively. The absorbance (bold line) spectrum was normalized to the value at 277 nm.

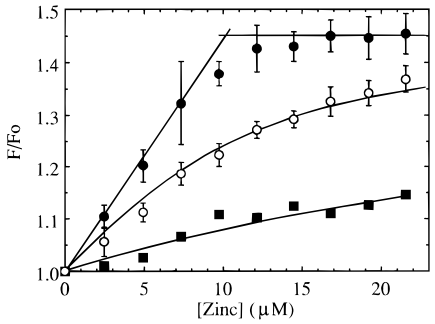

FIGURE 3: Tyrosine fluorescence enhancement upon addition of zinc aliquots to 10 μM peptide in 100 mM potassium glutamate, 5 mM DTT, buffered at the pH shown using a mix of 10 mM each acetic acid, PIPES, HEPES, Tris, and CHES. This buffer has nearly constant buffering capacity over a range from 4.5 to 9.5. The corrected fluorescence enhancement, F/F_o, from three titrations was averaged, and the standard deviations are shown by the error bars. Two straight lines were used to fit the data at pH 7.46 (filled circles). The data at pH 5.03 (open circles) and 9.50 (filled squares) were used to obtain $(F/F_o)_{max}$ and $K_{dissociation}$ by nonlinear least-squares fit. The fit constants were then used to derive the fit lines through the data.

of tyrosine and not tyrosinate (Lakowicz, 1983; Longworth, 1983). The quantum yield of the tyrosine in the metal-free peptide at pH 7.5 was 0.065. This value was less than half that for free tyrosine which has a quantum yield of 0.14 (Longworth, 1983) indicating that the tyrosine in the peptide was quenched. The addition of the zinc to the peptide caused a 1.46-fold enhancement in the emission intensity with no change to the spectral shape. The excitation spectral shape below 280 nm shifted slightly when the peptide bound zinc, possibly indicating more energy transfer from the phenylalanines to tyrosine.

Peptide−Zinc Binding Stoichiometry and Affinity. The fluorescence of the single tyrosine increased linearly as zinc was added to the peptide at pH 7.5 and reached saturation after 1 equiv zinc was added (Figure 3). Since the peptide bound nearly all of the zinc added, there was no free zinc present and it was not possible to use the fluorescence data to obtain an accurate equilibrium constant under these conditions. For example, when the pH 7.5 data was subjected to a nonlinear least squares fit, the fit dissociation constant was 0.10 ± 0.08 μM. The interaction was fully reversible by 3 mM EDTA, indicating that the complex was in equilibrium and that the peptide bound the zinc weaker than did EDTA.

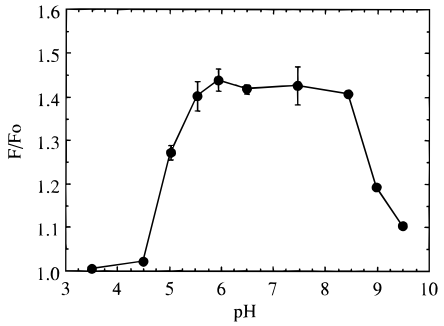

FIGURE 4: Peptide fluorescence enhancement caused by one zinc equivalent. The data is from titrations like those in Figure 3 except that the intensity shown is for 10 μM peptide and zinc acetate at each pH. The values represent the average, and the error bars represent the standard deviations from three titrations.

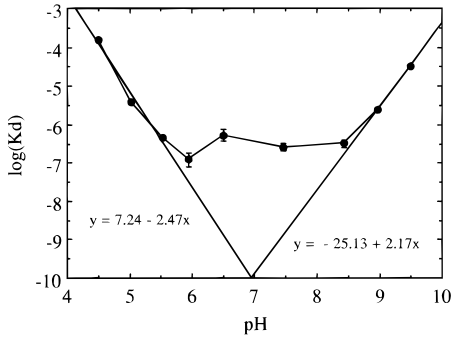

FIGURE 5: Zinc−peptide dissociation constant versus pH interpolation plot. The logarithm of dissociation constants obtained from nonlinear least-squares fit of data like those in Figure 3 were plotted versus pH. Two simple line fits were made to the low and high pH data which had yielded accurate constants.

To establish conditions under which the affinity could be measured, a zinc titration of the peptide was performed at pH's between 3.5 and 9.5 (Figure 3, most data not shown). When the fluorescence enhancement caused by 1.0 equiv of zinc was plotted versus pH (Figure 4), it revealed that zinc bound to the peptide stoichiometrically between pH 6.0 and 8.5. The average maximum fluorescence enhancement at these pH's was 48% ± 2%. This average value was used for data analysis outside this range. Data fitting indicated that the dissociation constants below pH 6 and above pH 8.5 had acceptably small standard deviations (less than 10% of the fit value) that they could be considered accurate (Figure 3). When the dissociation constants were plotted versus pH (Figure 5), it was possible to estimate the dissociation constants at the intermediate pH's by interpolation from the accurate values. From this type of analysis, the dissociation constant at pH 7.5 was in the range 10−100 nM. Next, the tyrosine environment was probed by analyzing the zinc effect on the tyrosine fluorescence: intensity pH dependence, lifetime, radiative and nonradiative rates, and collisional quenching effects.

Tyrosine Fluorescence Intensity pH Dependence. The pH profile of peptide fluorescence intensity provided information about the quenching effectiveness of protonatable groups near the tyrosine (Figure 6). The pH effect was similar whether it was the free peptide, the peptide with EDTA, or the peptide bound to zinc, indicating that zinc affected the tyrosine intensity independent of pH. When the pH dependence was fit by nonlinear least-squares fit to the sum of a minimal intensity F_{min} and two proton-sensitive species $F_i/(1 + 10^{(pH-pK)})$, good fits were obtained with only 2.7% error. The

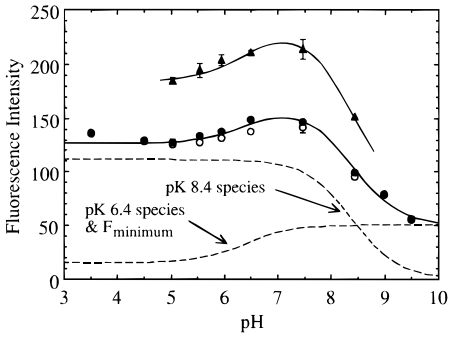

FIGURE 6: Fluorescence intensity pH profile for the free peptide (F_o, closed circles), peptide−zinc complex ($F_{saturation}$, closed triangles), and free peptide obtained after adding 3 mM EDTA to the peptide−zinc complex (F_o, open circles). Each value was determined in triplicate, and the standard deviations are shown by the error bars. For most values, the error was smaller than the symbol denoting the value. The F_o fit was generated using two one-proton pH equations as described under Results. The $F_{saturation}$ curve was obtained by multiplying the F_o fit by 1.46.

two protonatable species had p*K*'s of 6.4 ± 0.2 and 8.39 ± 0.05. The p*K* 6.20 species was a quencher when protonated, and the 8.40 species was a quencher when deprotonated. The relative intensity contributions of the species were $F_{min} = 50 \pm 1$, $F_{pK=6.4} = -30 \pm 2$, were $F_{pK=8.4} = 111 \pm 1$ indicating that the p$K = 8.4$ species was a more effective quencher than the p$K = 6.4$ species.

Peptide Tyrosine Fluorescence Photophysics. Given the 46% increase in tyrosine quantum yield when the peptide bound zinc, its lifetime was measured to determine the relative contributions of the radiative and sum of nonradiative rates. The single tyrosine in the free or zinc-bound peptide were well-described by triple exponentials as indicated by the goodness-of-fit values being about 3-fold less than for double exponential fits (Table 2). The three components of the free peptide lifetime data were averaged to yield 1.46 ns (Table 3). One of the three components of the zinc−peptide complex had a subpicosecond lifetime (Table 2). Such a short lifetime suggested that this component correlated to light scattering rather than to a radiating species. Even though aggregation was not visible in the cuvette following the 20-min measurement, in other experiments we found that the peptide became less soluble when it bound zinc. The average fluorescence lifetime for the peptide−zinc complex was 1.96 ns (= {0.22 × 3.29 ns + 0.29 × 0.95 ns}/{0.22 + 0.29}), indicating that the average lifetime was enhanced 1.34-fold upon binding zinc. This was nearly the extent to which the quantum yield had been enhanced. From this it could be concluded that when the peptide bound to zinc, the quantum yield and average lifetime were altered primarily because of a decrease in the average sum of nonradiative rate constants and not because of much change in the radiative rate constant (Table 3).

Peptide Tyrosine Fluorescence Extrinsic Quenching. Changes in the tyrosine solvent exposure were determined in studies with the extrinsic quenching agents acrylamide, iodide, and cesium. In theory, the collisional quenching constant for each agent can provide information about the collisional efficiency, molecular weight, and radius of the molecule to which the fluorophore is attached, and the fractional exposure of the fluorophore (Johnson & Yguerabide, 1985). Since the peptide does not change mass by much when it binds zinc, the constant should only be sensitive to the other two parameters. In addition, the collisional efficiency effect can be accounted for by dividing the constant by that for the quenching of fully exposed indole giving that ratio $k_{q,peptide}/k_{q,indole}$ which was related to the solvent exposure of the fluorophore.

Stern−Volmer plots of the acrylamide quenching data for free and zinc-bound peptide had significant upward curvature (data not shown) indicating that collisional and static quenching were taking place simultaneously. To account for this, the data were analyzed using a modified Stern−Volmer equation. Analysis indicated that neither the static quenching constant V nor the Stern−Volmer constant K_{SV} changed much when the peptide bound zinc (Table 4). Since the average tyrosine lifetime increased by 34% upon binding zinc, however, both $k_{q,peptide}$ and $k_{q,peptide}/k_{q,indole}$ were less in the peptide−zinc complex than in the free peptide, indicating a signficant decrease in tyrosine solvent exposure upon zinc binding.

The acrylamide static quenching of tryptophan is typically less than 3 M^{-1} (Eftink & Ghiron, 1976), but that for the peptide tyrosine was about 4.2 M^{-1}. The sphere-of-action model, used to interpret the static quenching constant, indicated that when acrylamide was within 11 Å of the tyrosine it was capable of static quenching. At 12 Å, the acrylamide need only bind to the outer surface of this folded peptide to be able to quench a completely buried tyrosine. Alternatively, such a large value for V suggested that the acrylamide was actually binding to the rather hydrophobic peptide.

The Stern−Volmer constant for cesium also did not change much when the peptide bound zinc. It was less effective than acrylamide because its quenching efficiency is 20% compared to acrylamide's 100% (Eftink & Ghiron, 1981). When the change in lifetime upon zinc binding and the lower cesium quenching efficiency effect were accounted for by calculating $k_{q,peptide}/k_{q,indole}$ (Table 4), it was found that the cesium ratios for both free and zinc-bound peptide were larger than for acrylamide. This could be explained by the accessible quencher collision site having a negative charge whether or not zinc was bound. The iodide quenching ratios (Table 4) confirmed that their was a slight negative charge near the tyrosine quencher entry site but also indicated that the binding of zinc made the site even more negatively charged than had the acrylamide or cesium ratios. For all three quenching agents, the quenching ratio was lower by 25%−40% for tyrosine in the zinc-bound form indicating that the tyrosine was protected from solvent upon zinc binding regardless of quencher.

Peptide Circular Dichroism Spectra. The effect of pH and zinc binding on polypeptide backbone structure and aromatic residue geometry was determined by far ultraviolet circular dichroism (Figure 7). When the potential contributions from the aromatic groups were ignored, all spectra indicated the presence of roughly equal amounts of random coil and beta strand structures. Changes in the circular dichroism spectra were more strongly dependent upon pH than on zinc binding (Figure 7). Even though at pH 3.0 the peptide had very low affinity for zinc (Figure 5), the pH 3.0 spectrum was not that of a random coil. The lower pH structure must not be capable of binding zinc. As the pH was raised from pH 3.0 to 7.2, the ellipticity values at each wavelength between 195 and 210 nm become less negative which may indicate a decrease in β strand structure. An

Table 2: Fluorescence Lifetimes of Primase Zinc Finger Peptide Tyrosine[a]

sample	χ^2 [b]	3-component fit						
		χ^2	a_1	τ_1 (ns)	a_2	τ_2 (ns)	a_3	τ_3 (ns)
free peptide	27	7.1	0.32	3.13	0.55	0.85	0.13	0.018
peptide−zinc complex	17	7.8	0.22	3.29	0.29	0.95	0.50	0.000

[a] All values were obtained as described under Experimental Procedures at 25 °C. The χ^2 residuals goodness-of-fit values were determined for 1-, 2-, and 3-component fits. The lifetimes and amplitudes for the best fit are shown. [b] 2-Component fit.

Table 3: Primase Zinc Finger Peptide Tyrosine Photophysics[a]

compound	ϕ	$<\tau>$ (ns)	$<k_r>$ (10^8 s^{-1})	$<\sum k_{nr}>$ (10^8 s^{-1})
N-acetyltyrosinamide	0.14[b]	1.47	0.95	5.3
free peptide	0.065	1.46	0.45	6.4
peptide−zinc complex	0.095	1.96	0.48	4.6

[a] The quantum yield ϕ was determined for each compound as described under Experimental Procedures. The amplitude-weighted average fluorescence lifetime $<\tau>$ for free peptide was calculated from the data presented under Table 2 and for the peptide−zinc complex as described under Results. The average radiative rate constant $<k_r>$ and the average sum of nonradiative rate constants $<\sum k_{nr}>$ were calculated using the quantum yields and lifetimes as described under Experimental Procedures. These rate constants must be considered underestimates by ∼10% because the quantum yields and lifetimes were determined at 30 and 25 °C, respectively. These underestimates do not alter the relative conclusions. [b] The quantum yield for for *N*-acetyltyrosinamide was from Longworth (1983).

Table 4: Collisional Quenching of Tyrosine in the Zinc Finger Peptide[a]

quenching agent	K_{SV} (M^{-1})	V (M^{-1})	$k_{q,peptide}$ (10^9 M^{-1} s^{-1})	$k_{q,peptide}/k_{q,indole}$
peptide				
acrylamide	3.67 ± 0.09	4.31 ± 0.06	2.51	0.35
cesium chloride	0.80 ± 0.01		0.55	0.50
potassium iodide	2.34 ± 0.04		1.60	0.25
peptide + zinc				
acrylamide	3.59 ± 0.05	4.11 ± 0.04	1.83	0.26
cesium chloride	0.81 ± 0.01		0.41	0.37
potassium iodide	1.85 ± 0.03		0.94	0.15

[a] The tyrosine fluorescence was monitored by exciting at 280 nm and emitting at 305 nm. Each quencher titration was performed in triplicate using 10 μM peptide with or without an equivalent of zinc acetate. These collisional quenching rate constants $k_{q,peptide}$ must be considered underestimates by ∼10% because the Stern−Volmer constants, lifetimes, and indole quenching constants were determined at 30, 25, and 25 °C, respectively. These underestimates do not alter the relative conclusions.

alternative explanation was that there was a change in tyrosine geometry. This was an especially likely interpretation because the helical content was predicted to be low so that even small changes in the other ellipticities can be observed (Manning & Woody, 1989).

At pH 7.2, the spectrum was shifted higher by about 2 nm when the peptide was bound to zinc. The far ultraviolet absorbance spectrum of the peptide also shifted higher by about 1.5 nm when the peptide bound to 1 equiv of zinc (data not shown) possibly indicating a change in the electronic environment of dichroically absorbing species. Regardless of the interpretation, the small spectral change indicated that the peptide secondary structure and tyrosine geometry did not change much when the peptide bound zinc.

Cobalt−Peptide Spectrum and Affinity. Information about metal ligation and geometry were obtained by metal substitution. Since zinc(II) and cobalt(II) have similar ionic radii

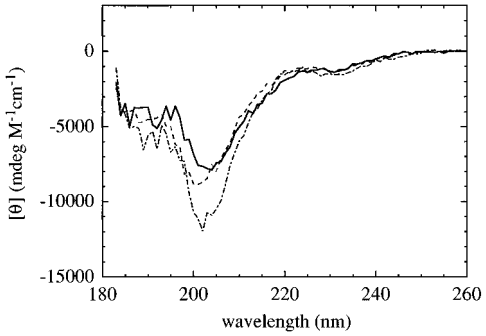

FIGURE 7: Far-ultraviolet circular dichroism spectra of the peptide. The peptide spectra at pH 7.2 were determined with 0.9 equiv of zinc (solid line) or without zinc (dashed line) and at pH 3.0 (dashed and dotted line) without zinc.

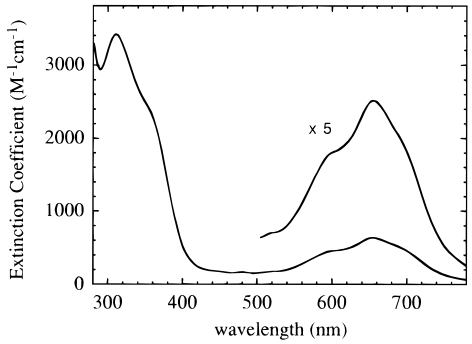

FIGURE 8: Visible extinction spectrum of the cobalt−peptide complex. The peptide (58 μM) in 50 mM HEPES, pH 7.5, was mixed with 88 μM cobalt chloride to make the complex. Higher amounts of cobalt did not improve the spectrum but did cause sample opacity. The resulting absorbance spectrum was divided by the peptide concentration to obtain the extinction spectrum. The inset shows extinctions from 500 to 800 nm factored by 5.

and ligation preferences, the catalytic activity of cobalt-substituted zinc enzymes is usually satisfactory (Vallee & Galdes, 1984). What makes cobalt(II) useful as a substitute is that it is optically active whereas zinc is not. The visible absorption spectrum of tetrahedral, high-spin cobalt(II) is sensitive to the geometry, number, and type of ligating atoms. When saturating amounts of cobalt were added to a pH 7.5 solution lacking DTT of the primase zinc binding peptide, a visible absorption spectrum characteristic of cobalt tetrahedrally coordinated by three cysteines and one histidine was obtained (Figure 8) (Guo et al., 1995; Klemba & Regan, 1995; Krizek et al., 1991, 1993). The thiolate-to-cobalt charge transfer electronic transition at 311 nm had an extinction coefficient of 3418 M^{-1} cm^{-1}. Assuming that there were three cysteinate−cobalt bonds, the average extinction per bond would be 1139 M^{-1} cm^{-1}, similar to values established for other thiolate−cobalt bonds (900−1400 M^{-1} cm^{-1}).

The ligand field transition region of the spectrum (λ = 500−800 nm) exhibited a shoulder at 602 nm and a maximum at 655 nm. The 655 nm peak was of similar

energy to other cobalts coordinated by three sulfur and one nitrogen. For comparison, four-sulfur coordination results in a peak at about 750 nm whereas two-sulfur and two-nitrogen coordination result in a peak at about 620 nm. The maximum extinction was 635 M^{-1} cm^{-1} which was at the high end of the typical range for tetrahedral cobalt−peptide complexes (200−800 M^{-1} cm^{-1}). In shape and intensity, the primase peptide−cobalt spectrum was most similar to that reported for cobalt-substituted bacteriophage T4 gene 32 protein which coordinates cobalt using one histidine and three cysteinates (Giedroc et al., 1992; Qiu & Giedroc, 1994).

When cobalt was titrated into a 64 μM peptide solution in 50 mM HEPES, pH 7.5 buffer (data not shown), the absorbances at 311 and 655 nm increased proportionally until the cobalt concentration equaled that of the peptide and then the absorbance increased only slightly. This indicated that the cobalt−peptide dissociation constant was less than 10 μM and that the cobalt was binding stoichiometrically to the peptide. Because the extinction coefficients were small, it was not possible to use lower concentrations of peptide to carry out the titrations to obtain the dissociation constant. When 19 μM zinc acetate was added to the cobalt−peptide complex in which the cobalt was present in 3-fold excess, the absorbances decreased by about 30%. This indicated that the zinc had substantially higher affinity for the peptide than did the cobalt. The solution became opaque when higher amounts of zinc were added, indicating that high metal concentrations caused the formation of an insoluble complex.

DISCUSSION

Amino acid sequence analysis indicates that the putative bacterial primase "zinc finger" (Ilyina et al., 1992) motif is highly conserved and that it may be in a zinc finger family shared only with eukaryotic viral primase zinc fingers. A search in a protein database indicated that there was no precedent for metal binding by the first half of the motif, CXXH, but that there was extensive evidence for metal chelation by the second half of the motif, (F/Y)XCXXC. We show here that a peptide with the sequence of the putative zinc binding portion of bacterial primase is capable of binding zinc specifically and reversibly. Even though the affinity of the peptide for zinc ($K_d \approx 10-100$ nM) is lower than that of the entire primase enzyme ($K_d < 1$ pM) (Griep & Lokey, 1996), the affinity is quite high and provides strong evidence that this sequence represents a new zinc binding motif. The peptide−cobalt absorption spectrum confirms the sequence analysis prediction that the metal is tetrahedrally bound by three thiolates and one histidine nitrogen.

Even though the peptide has zinc binding specificity, the circular dichroism data indicates that the peptide folds into a secondary structure even without the zinc. The role of the zinc is not to induce structure but perhaps to stabilize it. Indeed, the peptide readily binds zinc when it is freshly dissolved in degassed buffer or water, but after a few days storage it was necessary to add a mild reductant to the stock peptide solution to restore zinc binding (data not shown). One of the roles of the zinc may be to prevent disulfide bond formation of the closely placed cysteines in the folded structure, the same role as in the full enzyme (Griep & Lokey, 1996).

In a previous study, we found that reduced apoprimase had as much enzymatic activity as the native enzyme (Griep & Lokey, 1996). We suggested that there might be contacts with portions of primase distant from the zinc finger region that stabilize its secondary structure even in the absence of zinc. We demonstrate here that these long-range contacts do not need to be hypothesized to explain why the apoenzyme retained its activity. Even though the ability of primary structure to determine secondary structure has been well-established (Anfinsen, 1973), zinc finger peptides seem to represent a particularly favorable case; their relatively modest lengths are often associated with specific structures and functions (Klug & Schwabe, 1995; Schmiedeskamp & Klevit, 1994; Vallee & Auld, 1993). Other examples of single-zinc binding peptides that have structure or function in the absence of bound zinc are the one derived from HIV-1 nucleocapsid protein which retains structure and functionality (Delahunty et al., 1992); the one derived from isoleucyl-tRNA synthetase which retains structure but not full functionality (Glasfeld et al., 1996); and a classical zinc finger consensus-derived peptide which adopts partial structure (Eis & Lakowicz, 1993).

Far-ultraviolet circular dichroism can provide a sensitive measure of backbone geometry because it is strongly correlated to polypeptide secondary structure (Johnson, 1990). When there is low helical content and high aromatic or disulfide content, however, the observed ellipticities cannot be used for structure predictions in the usual manner of assuming that it is the sum of fractional structure contributions. The aromatic and disulfide ellipticities become significant and have magnitudes that are difficult to predict even when their actual geometries and environments are known (Manning & Woody, 1989; Mark et al., 1995; Woody, 1994). The primase zinc finger peptide does not seem to have helical structure but it does have five phenylalanines and one tyrosine among its 35 residues. Sequence analysis and cursory structure prediction based on the circular dichroism data indicate that primase zinc fingers are probably composed of β strand and random coil. The circular dichroism spectra indicate that the free and zinc-bound peptides have similar secondary and aromatic residue structures. The small spectral shift that does occur upon zinc binding is at a tyrosine absorption peak (200 nm) (Hooker & Schellman, 1970) and may be explained by a slight change in tyrosine geometry or environment when the peptide binds zinc rather than as a change in polypeptide structure.

The collisional quenching constant ratios $k_{q,peptide}/k_{q,indole}$ for acrylamide, cesium, and iodide indicate that the tyrosine is mostly buried within the free polypeptide. The ratios for iodide and cesium compared to that for acrylamide indicate that there is a slight negative charge at the quencher entry site. All three ratios decrease by 25% when the peptide binds zinc, suggesting that zinc binding reduces tyrosine quencher accessibility somewhat. Analysis of the acrylamide collisional quenching ratios indicate that the actual percentage of accessible tyrosine [see Figure 2B of Johnson and Yguerabide (1985)] decreases from about 20% to about 12% in response to zinc binding. This complements the circular dichroism data to indicate that the tyrosine is buried in a peptide that has considerable structure with or without zinc.

The tyrosine fluorescence intensity is strongly influenced by protonatable groups with pK's of 6.4 and 8.4. Since the same pH profile was observed with and without bound zinc, neither of these species can be the zinc ligating cysteines or histidine. The ability of the protonatable species to quench

the tyrosine depends on both their intrinsic quenching efficiency and ability to make favorable quenching contact with the tyrosine. The p*K* 6.2 species is likely to be one or more of the non-zinc-ligating histidines while the p*K* 8.4 species could be either a lysine with a shifted p*K* or the amino terminus. Protonated histidine is an efficient quencher of tryptophan because it is an efficient electron scavenger (Shinitzky & Goldman, 1967; Steiner & Kirby, 1969). The most obvious candidate to be the quenching histidine is the one that immediately follows the tyrosine in the linear sequence even though it could just as easily be a histidine located far away in the linear sequence as has been observed in the peptide anantin (Vos & Engelborghs, 1994) and the protein barnase (Loewenthal et al., 1991). Unprotonated lysine quenches tyrosine by acting as a proton and then an electron acceptor (Feitelson, 1964; Mayer et al., 1978). The two lysines immediately adjacent to glutamates would be predicted to have a lower than usual ϵ-amine p*K*'s and would be better candidates than the amino-terminal lysine which would be predicted to have a higher ϵ-amine p*K*. Since the pH profile does not change when the peptide binds zinc, it indicates that there is no change in protonatable species in the immediate environment of the tyrosine. This would exclude the zinc ligating residues from being in the immediate sphere of the tyrosine because their ability to act as quenchers would be pH dependent.

The final issue to address is the cause of the zinc-dependent decrease in a tyrosine nonradiative rate constant that results in a 46% enhancement of the tyrosine quantum yield and a 34% enhancement of the average lifetime. Since static quenching is associated with changes to the radiative process and collisional quenching with a nonradiative process, the simplest explanation is that zinc binding relieves an intramolecular collisional quenching process. For the primase zinc finger peptide, this may involve either direct ligation to the quenching residues or immobilization of the quenching residues upon zinc binding. The zinc ligating residues would be likely candidates in this process because protonated histidine and cysteine are effective collisional quenchers (Harris & Hudson, 1990; Steiner & Kirby, 1969) and because all of the peptide cysteines but only one of the four histidines are involved in zinc ligation. Upon binding zinc, the three cysteines deprotonate, bind to a divalent zinc, and alter the net charge at the metal binding site from neutral to −1. Even though tyrosine solvent accessibility decreases from about 20% to 12% when the peptide binds zinc, there is only a small change in the iodide and cesium tyrosine quenching efficiencies relative to that for acrylamide. Therefore, zinc is able to reduce tyrosine accessibility but is not close enough to alter its electrostatic environment. These data are consistent with the zinc ligating residues as being the cause of the low lifetime and quantum yield of the free peptide and yet not being close enough to cause pH-dependent changes to the tyrosine fluorescence intensity.

ACKNOWLEDGMENT

We heartily thank Todd Wells for changing the lamp on the circular dichroism spectrophotometer and cleaning its delicate mirrors so that our spectra were the best they could be.

REFERENCES

Anfinsen, C. B. (1973) *Science 181*, 223−230.
Berg, J. M. (1995) *Acc. Chem. Res. 22*, 4705−4710.
Bernstein, J. A., & Richardson, C. C. (1988) *Proc. Natl. Acad. Sci. U.S.A. 85*, 396−400.
Bertini, I., & Luchinat, C. (1994) in *Bioinorganic Chemistry* (Bertini, I., Gray, H. B., Lippard, S. J., & Valentine, J. S., Eds.) pp 37−106, University Science Books, Mill Valley, CA.
Burton, Z. F., Gross, C. A., Watanabe, K. K., & Burgess, R. R. (1983) *Cell 32*, 335−349.
Chen, R. F. (1967) *Anal. Lett. 1*, 35−42.
Chou, P. Y., & Fasman, G. D. (1974) *Biochemistry 13*, 211−215.
Delahunty, M. D., South, T. L., Summers, M. F., & Karpel, R. L. (1992) *Biochemistry 31*, 6461−6469.
Eftink, M. R. (1991) in *Topics in Fluorescence Spectroscopy, Volume 2: Principles* (Lakowicz, J. R., Ed.) pp 53−126, Plenum Press, New York.
Eftink, M. R., & Ghiron, C. A. (1976) *J. Phys. Chem. 80*, 486−493.
Eftink, M. R., & Ghiron, C. A. (1981) *Anal. Biochem. 114*, 199−227.
Eis, P. S., & Lakowicz, J. R. (1993) *Biochemistry 32*, 7981−7993.
Feitelson, J. (1964) *J. Phys. Chem. 68*, 391−397.
Giedroc, D. P., Qiu, H., Khan, R., King, G. C., & Chen, K. (1992) *Biochemistry 31*, 765−774.
Glasfeld, E., Landro, J. A., & Schimmel, P. (1996) *Biochemistry 35*, 4139−4145.
Griep, M. A. (1995) *Indian J. Biochem. Biophys. 32*, 171−178.
Griep, M. A., & Mesman, T. N. (1995) *Bioconjugate Chem. 6*, 673−682.
Griep, M. A., & Lokey, E. R. (1996) *Biochemistry 35*, 8260−8267.
Grompe, M., Versalovic, J., Koeuth, T., & Lupski, J. R. (1991) *J. Bacteriol. 173*, 1268−1278.
Group, G. C. (1994) *Program Manual for the Wisconsin Sequence Analysis Package, Version 8*, Genetics Computer Group, 575 Science Drive, Madison, WI.
Guo, J., Wang, S., Dong, J., Qiu, H., Scott, R. A., & Giedroc, D. P. (1995) *J. Am. Chem. Soc. 117*, 9437−9440.
Harris, D. L., & Hudson, B. S. (1990) *Biochemistry 29*, 5276−5285.
Hooker, T. M., Jr., & Schellman, J. A. (1970) *Biopolymers 9*, 1319−1348.
Ilyina, T. V., Gorbalenya, A. E., & Koonin, E. V. (1992) *J. Mol. Evol. 34*, 351−357.
Johnson, D. A., & Yguerabide, J. (1985) *Biophys. J. 48*, 949−955.
Johnson, C. W., Jr. (1990) *Proteins 7*, 205−214.
Klemba, M., & Regan, L. (1995) *Biochemistry 34*, 10094−10100.
Klug, A., & Schwabe, J. W. R. (1995) *FASEB J. 9*, 597−604.
Kornberg, A., & Baker, T. A. (1992) *DNA Replication*, 2nd ed., W. H. Freeman and Company, New York.
Krizek, B. A., Amann, B. T., Kilfoil, V. J., Merkle, D. L., & Berg, J. M. (1991) *J. Am. Chem. Soc. 773*, 4518−4523.
Krizek, B. A., Merkle, D. L., & Berg, J. M. (1993) *Inorg. Chem. 32*, 937−940.
Lakowicz, J. R. (1983) *Principles of Fluorescence Spectroscopy*, Plenum Press, New York.
Lakowicz, J. R., Laczko, G., & Gryczynski, I. (1987) *Biochemistry 26*, 82−90.
Laws, W. R., Ross, J. B. A., Wyssbrod, H. R., Beechem, J. M., Brand, L., & Sutherland, J. C. (1986) *Biochemistry 25*, 599−607.
Loewenthal, R., Sancho, J., & Fersht, A. R. (1991) *Biochemistry 30*, 6775−6779.
Longworth, J. W. (1983) *NATO ASI Ser., Ser. A 69*, 651−686.
Manning, M. C., & Woody, R. W. (1989) *Biochemistry 28*, 8609−8613.
Marians, K. J. (1992) *Annu. Rev. Biochem. 61*, 673−719.
Mark, B. L., Terwilliger, T. C., Vaughan, M. R., & Gray, D. M. (1995) *Biochemistry 34*, 12854−12865.
Mayer, R., Gauduchon, P., Spach, G., & Wahl, P. (1978) *Biopolymers 17*, 337−360.
Mendelman, L. V., Beauchamp, B. B., & Richardson, C. C. (1994) *EMBO J. 13*, 3909−3916.
Miller, J., McLachlan, A. D., & Klug, A. (1985) *EMBO J. 4*, 1609−1614.

Parker, C. A., & Rees, W. T. (1960) *Analyst 85*, 587−600.
Qiu, H., & Giedroc, D. P. (1994) *Biochemistry 33*, 8139−8148.
Sasagawa, T., Okuyama, T., & Teller, D. C. (1982) *J. Chromatogr. 240*, 329−340.
Schmiedeskamp, M., & Klevit, R. E. (1994) *Curr. Opin. Struct. Biol. 4*, 28−35.
Schuaerte, J. A., & Gafni, A. (1989) *Biochemistry 28*, 3948−3954.
Shinitzky, M., & Goldman, R. (1967) *Eur. J. Biochem. 3*, 139−144.
Stamford, N. P. J., Lilley, P. E., & Dixon, N. E. (1992) *Biochim. Biophys. Acta 1132*, 17−25.
Steiner, R. F., & Kirby, E. P. (1969) *J. Phys. Chem. 73*, 4130−4135.
Stern, O., & Volmer, M. (1919) *Phys. Z. 20*, 183−188.
Swart, J. R., & Griep, M. A. (1995) *Biochemistry 34*, 16097−16106.
Vallee, B. L., & Galdes, A. (1984) *Adv. Enzymol. 58*, 283−430.
Vallee, B. L., & Auld, D. S. (1993) *Acc. Chem. Res. 26*, 543−551.
Versalovic, J., & Lupski, J. R. (1993) *Gene 136*, 281−286.
Vos, R., & Engelborghs, Y. (1994) *Photochem. Photobiol. 60*, 24−32.
Woody, R. W. (1994) *Eur. Biophys. J. 23*, 253−262.
Wu, C. A., Zechner, E. L., Reems, J. A., McHenry, C. S., & Marians, K. J. (1992) *J. Biol. Chem. 267*, 4074−4083.
Zechner, E. L., Wu, C. A., & Marians, K. J. (1992) *J. Biol. Chem. 267*, 4045−4053.

BI9612778